WS 3/4/06

Adam

Chapter 9

Fit Method

With the obtained differential event shape distributions and the event shape means, the data can now be compared to pQCD plus Power Correction predictions. The total QCD prediction for the value of an event shape can be expressed as a sum of the parton-level prediction from an NLO integration program and a power-law correction for hadronization (Equation (2.18)). After fitting the theory to the data, extractions of the free parameters, $\alpha_s(M_Z)$ and $\overline{\alpha_0}(\mu_I)$, together with an examination of the systematic and theoretical uncertainties enable a ~~discussion of the validity of~~ evaluation of the Power Correction model.

9.1 Fits to the Means

9.1.1 Fit Procedure

what remaining variables?

To extract α_s and $\overline{\alpha_0}$ from the remaining variables, it is necessary to compare the NLO + PC prediction to the data ~~at an arbitrary point in~~ for values of α_s and $\overline{\alpha_0}$ space. The NLO prediction is determined using the parameterization discussed in Section 5, while

the power correction is calculated according to (2.23). A χ^2 can then be determined:

$$\chi^2(\alpha_s, \overline{\alpha_0}) = \sum_i \left(\frac{t_i - m_i}{\sigma_i} \right)^2 \tag{9.1}$$

with measured data

$$m_i = \langle F \rangle_{data,i} \tag{9.2}$$

and theory

$$t_i = \langle F \rangle_{NLO,i} + \langle F \rangle_{PC,i} \tag{9.3}$$

where the sum is over the fitted bins, i. The term σ_i is found by combining in quadrature the statistical errors in the data and in the NLO predictions. The contributions from the parameterized NLO prediction is determined from the statistical errors in the input distributions, taking into account correlations between c_1 and c_2 ((5.10)). The power correction is not determined statistically, so is assumed to have no error at this stage. The program MINUIT is used to perform a minimization of the χ^2, and a best fit of the two free parameters is determined.

9.1.2 Systematic Errors

So far, only the statistical errors have been incorporated into the χ^2 minimization of the fit of the QCD prediction to the data. There are two methods used to account for the systematic errors in the fit and extraction of free parameters. These two methods [44] are the *offset method*, and the *Hessian method*. Both are named from options in the MINUIT minimization program.

Offset Method The offset method is fairly straight forward. In the offset method, the fit is performed once for each systematic check. The deviation from the central

value of the fit can then be determined, and added in quadrature to give an estimate of the total systematic error. This usually results in a conservative estimate of the systematic errors. A further disadvantage is that the χ^2 of the fit includes only the statistical error, making it difficult to judge the overall quality of the fit.

Hessian Method The Hessian method incorporates both statistical and systematic errors by constructing a full error matrix. The fit is carried out as before, but the χ^2 distribution is re-expressed as

$$\chi^2 = \sum_i \left(\frac{t_i - m_i}{\sigma_i}\right)^2 - \boldsymbol{B}\boldsymbol{A}^{-1}\boldsymbol{B} \tag{9.4}$$

where

$$B_k = \sum_i \Delta_{ik}(m_i - t_i)/\sigma_i^2 \tag{9.5}$$

$$A_{kl} = \delta_{kl} + \sum_i \Delta_{ik}\Delta_{il}/\sigma_i^2 \tag{9.6}$$

and Δ_{ik} is the systematic error on a point i due to source k. In this χ^2 expression, all the systematic effects are contained in the term $\boldsymbol{B}\boldsymbol{A}^{-1}\boldsymbol{B}$, so that, were there no systematic errors, only the first term, identical to equation (9.1), would remain. In general, this method requires the matrix $\boldsymbol{A}$ to be inverted only once, but the σ_i include a contribution from the theory error, so $\boldsymbol{A}$ must be inverted every iteration. To keep this process as simple as possible, only the three dominant systematic effects are included, namely the ZUFO acceptance, ZUFO correction, and HERWIG correction.

The parameter values obtained by the offset and Hessian methods will typically be different, but should be consistent within the error estimates. The Hessian method tends to give smaller error estimates. It also has the advantage that the χ^2 includes

the systematic effects and can therefore be used to asses the quality of the fit, and to plot an estimator of the total statistical $\oplus$ systematic error contours.

9.2 Fits to the Differential Distributions

With the statistics offered by the 98-00 ZEUS data set, it is now possible to study the event shape spectra, rather than just the mean values. This is a more powerful technique. Mean event shapes include contributions from the full range of the distributions, but the theory is not expected to be accurate in all regions. The lack of terms beyond NLO causes a deficit of very broad events and an excess of strongly collimated events. Therefore, the theory does not match the data at each end of the distributions. By studying the differential distributions, one can identify regions in phase space where the model is performing well, and restrict the fits to these regions. The missing higher-order, resummation terms [44] still make small, but significant, contributions, even in this restricted phase space. However, it is still of interest to study NLO only.

A similar procedure to that used in fitting the means is used here, though the problem is somewhat more complex. As before, NLO calculations are made at five different values of α_s, using the CTEQ4A series. Fewer kinematic bins are usable in the differential distribution fits. Only bins 6-10 (Table 9.1), i.e. $\langle Q \rangle > 29\,\text{GeV}$, are used, since the calculations fail to describe the shapes of the distributions at lower Q. As with the means, y_2 and K_{OUT} are not fitted.

Fitting the differential distributions involves sliding the NLO predicted curves across the data spectra until a best fit is found. The NLO curves are calculated at a finite number of points, so it is therefore necessary to interpolate accurately between

points to find the NLO predictions at an arbitrary point in the range (see Section 5.3.2). Before the QCD fit is performed, a 9th-order Chebyshev polynomial [44] is fitted to each of the fitted shape distributions (five values of α_s and five kinematic bins). The Chebyshev fits are performed using curve and surface fitting routines from the NAG numerical libraries [44]. Since polynomials may struggle to fit distributions varying over orders of magnitude, the $\log_e$ of the distribution is fitted.

In addition, to ensure the correct upper limit to the distribution after non-perturbative corrections, as discussed in Section 5.4.2, a term of the form $1 - \left(\frac{V}{V_{\max}}\right)^{p_s}$ is also used in DISRESUM. The resummation can be expressed in terms of a rescaled variable, $1/x_L V$, instead of $1/V$, where x_L is a logarithmic rescaling factor [?]. The values of p, p_s and x_L are set by default to 1 and are varied to estimate the theoretical uncertainties of the method.

For the differential distributions, the NLO was matched to the NLL using DISRESUM and corrected by the the power correction following (2.26). For each observable the fit was performed using MINUIT [?, 45] to call DISRESUM with $\alpha_s(M_Z)$ and $\overline{\alpha_0}$ taken as free parameters.

The range of points used in the fits to the differential distribution has been defined individually for each shape variable and each Q^2 range. The ranges are limited by the requirements that the pQCD predictions should be well defined within the bin used in the fit and that the range used should not extend above the leading-order (LO) upper limit for the variable. The first requirement was based on the ratio (NLL + NLO + PC)/(NLL + NLO); bins were omitted at low values of the shape variable when the ratio showed a rapid fall with decreasing shape variable since clearly the

power correction is ill-defined in this region. Also the range $0.8 < F/F_{\max} < 1$ was excluded from the fit for $1 - T_\gamma$, B_γ and M, where the LO upper limit is equal to $F_{\max}$, due to large sensitivity to the modification effect.

The final ranges are summarized in Table 9.2. Since the theoretical predictions for differential distributions are reliable only at high values of Q^2, the fit was restricted to $Q^2 > 320\,\mathrm{GeV}^2$.

A χ^2 for an event shape F, measured in kinematic bins, i, and differential bins, j, is defined

$$\chi^2 = \sum_i \sum_j \left(\frac{m_{i,j} - t_{i,j}}{\sigma_{i,j}}\right)^2 \tag{9.7}$$

with measured data

$$m_{i,j} = \frac{1}{N(i)} \frac{dn(i,j)}{dF} \left[F_{measured}(j)\right] \tag{9.8}$$

and theory prediction

$$t_{i,j} = \frac{1}{N_{NLO}(i)} \frac{dn_{NLO}(i,j)}{dF} \left[F_{NLO}(j) - F_{PC}(i,j)\right] \tag{9.9}$$

explain

Each data point is compared to a corresponding theory prediction, calculated by sliding the NLO distribution a distance in phase space equal to the power correction term. The values of $t_{i,j}$ are determined by evaluating the predetermined Chebyshev polynomials for each distribution at the appropriate value of $F_{eval} = F_{NLO} - F_{PC}$. This is done for each value of α_s, and an interpolation in α_s is then carried out using a straight-line fit. Since the distributions are not linear over the width of the bins, simply evaluating at the center point of the data bin would not give an accurate value. The sequence of double interpolations is therefore carried out at eleven points over the width of each differential bin in the data, and the results are averaged to give the final $t_{i,j}$. $\sigma_{i,j}$ is the error on the data point, the interpolated NLO errors being insignificant.

Thus, the χ^2 is dependent on both $\alpha_s(M_Z)$ and $\overline{\alpha_0}$. MINUIT is used to minimize this function and best fit values of the two parameters are determined. Systematic uncertainties are then calculated, ~~as for~~ the mean fits. in the same way as for

9.3 Results

9.3.1 Mean values

The mean values of the event shape variables are compared with the ARIADNE predictions in Fig. 9.1. In general, there is a good agreement between data and MC. However the MC tends to overestimate the shape variables at low Q^2; this is especially marked for M^2. The ARIADNE predictions at the parton level are also shown. The difference between the hadron and parton level demonstrates the contribution from the hadronization process, as implemented in ARIADNE. Since the parton level of ARIADNE is not well defined [?], this should be taken as indicative only.

The mean values of the event shape variables $(1-T_T)$, B_T, M^2, C, $(1-T_\gamma)$ and B_γ as a function of Q were fitted by varying α_s and $\overline{\alpha_0}$ to the sum of an NLO term obtained from DISASTER++, plus the power correction as given by Equation (2.23)). The data and fit results are shown in Fig. 9.2.

For all variables the theory fits the data well. For $(1-T_\gamma)$, the best fit results in a negative power correction, whereas theory would suggest a power correction equal to that found for $(1-T_T)$.

The extracted values $(\alpha_s(M_Z), \overline{\alpha_0})$ are shown in Fig. 9.3 and in Table 9.3 and Table 9.4. The contours on the plot represent one standard deviation errors, corresponding to about 30% confidence level (CL), as well as the 95% CL regions based on

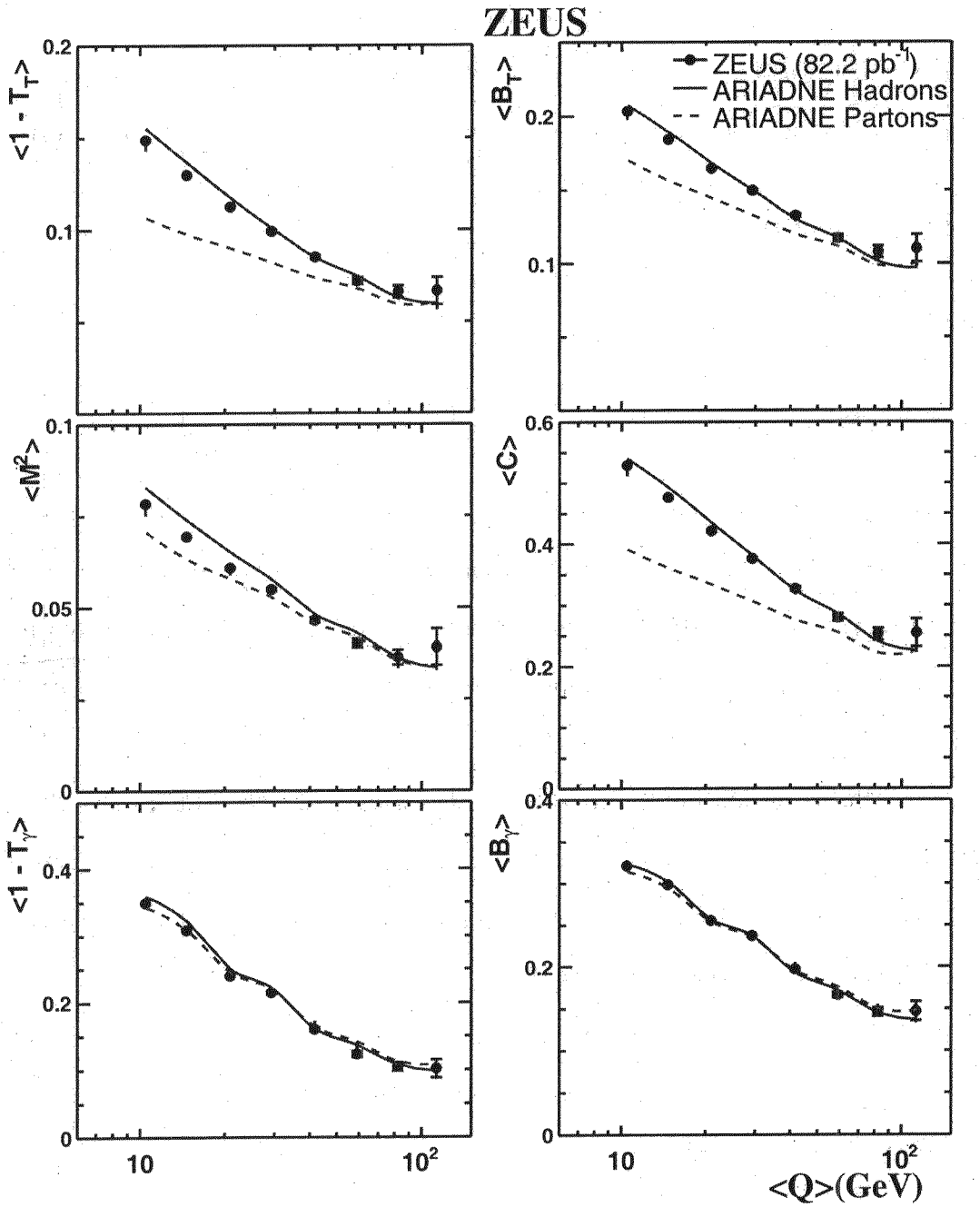

Figure 9.1: Mean event shapes compared to hadron- and parton-level ARIADNE mean event shape values.

the fit errors as calculated using the Hessian method. The theoretical uncertainties are not shown but are given in the tables, since they result in a correlated shift to all fit results. The current world average, $\alpha_s(M_Z) = 0.1182 \pm 0.0027$ [46], is also shown.

The $\overline{\alpha_0}$ values are in good agreement with those previously published [7], but somewhat lower than those obtained by the H1 and e^+e^- experiments. The values of α_s obtained from fits to $(1 - T_T)$, B_γ, C and M^2 are roughly consistent with each other. However, fits to B_T and $(1 - T_\gamma)$ give values of α_s which are inconsistent with the values obtained with the other variables, as already observed in the earlier ZEUS measurement. Need to comment here on this: why does this not cast entire measurement in doubt?

Table 9.3 and Table 9.4 show that the theoretical uncertainties are substantial and strongly correlated between variables. For α_s, the dominant uncertainty is that due to variation of the renormalization scale. What is special about B_T and $1-T_\gamma$?

The PDF uncertainty was evaluated by replacing the CTEQ4 PDFs by the MRS99 set. With the exception of $(1 - T_\gamma)$, the changes in the fitted $(\alpha_s(M_Z), \overline{\alpha_0})$ are of the order of the Hessian fit error. For $(1 - T_\gamma)$, the power correction becomes positive and the fitted values of $\alpha_s(\overline{\alpha_0})$ change to 0.1285(0.3541), values that are in closer agreement with the other variables. Of note is the uncertainty introduced by the variation of the scale μ_I.

If the model were robust, the fitted values of α_s would be independent of μ_I. However a dependence on μ_I is clearly evident in the Tables. It may be concluded that the inconsistency of the fitted α_s values, and their dependence on μ_I, demonstrate that the power-correction model does not consistently describe the mean shape variables in DIS. In view of these problems, no average $(\alpha_s(M_Z), \overline{\alpha_0})$ values are given.

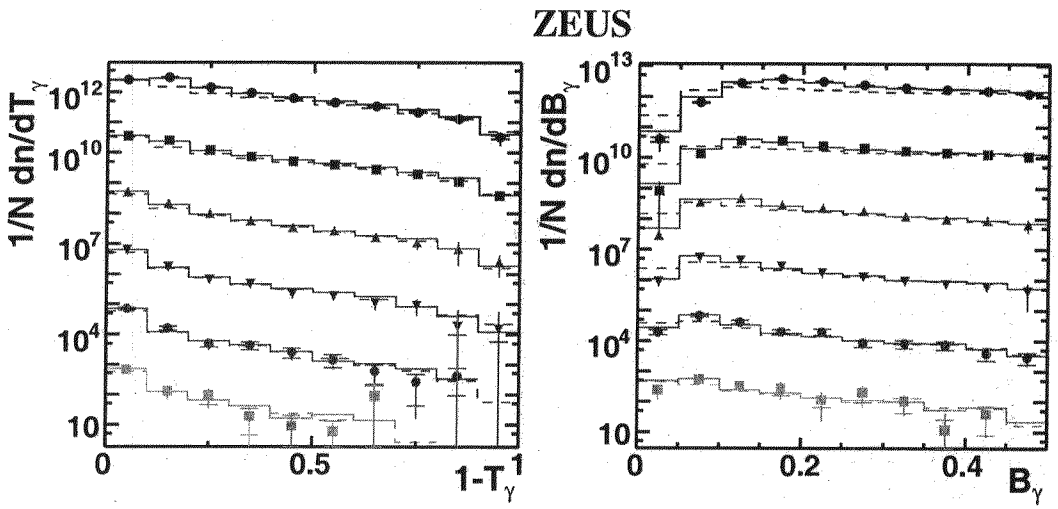

Figure 9.5: Comparisons of hadron- and parton-level ARIADNE Monte Carlo to hadron-level differential data in five different kinematic bins.

line). With the reservation stated above, the difference between the hadron and parton levels for ARIADNE can be taken as illustrative of the hadronization correction. These corrections can be seen to be negligible for y_2 but significant for K_{OUT}.

The differential distributions for $(1 - T_\gamma)$, B_γ, M^2, C and $(1 - T_T)$ have been fitted with NLL + NLO + PC calculations as shown in Fig. 9.6 and Fig. 9.7. The solid (dashed) bars show the bins that were used (unused) in the fit as described in Section 9.2.

reference or explain matching here and need for it.

Theoretically, it is unclear which matching technique is best. All have been studied and the results of fitting α_s and $\overline{\alpha_0}$ are shown in Fig. 9.8 and Table 9.7 and Table 9.8 for the six matching options. The χ^2 of the fits does not depend significantly on the form of matching used. M2mod matching has been chosen for the central analysis in view of the minimal dispersion of α_s and $\overline{\alpha_0}$ for this type of matching.

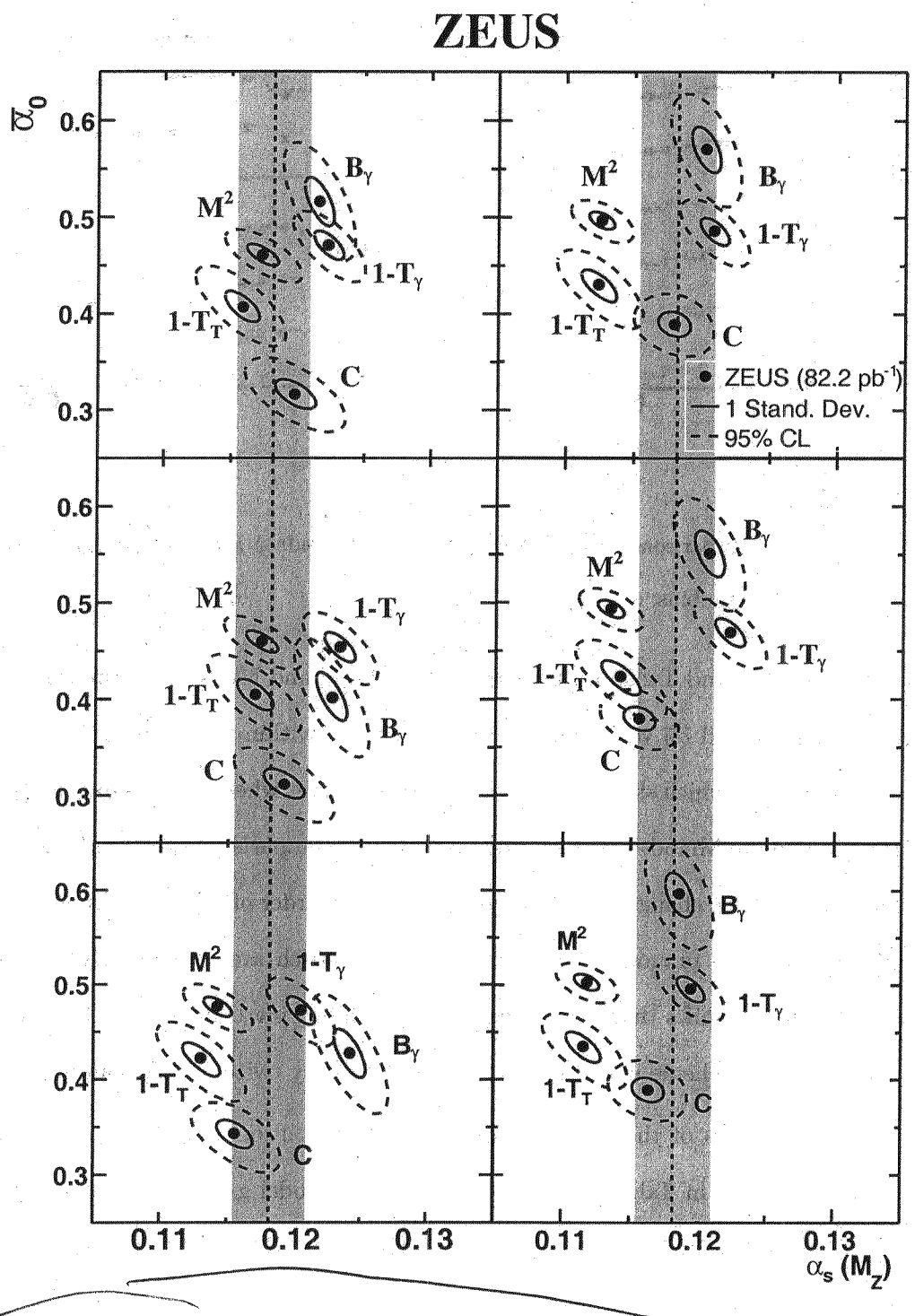

Figure 9.8: Contour plots showing values of extracted free parameters, $(\alpha_s(M_Z), \overline{\alpha_0})$, for fits to the differential distributions using different matching schemes.

variables the fit is less good with the χ^2/dof lying in the range 3-5. The fitted α_s values are consistent with the world average. With the exception of C, the $\overline{\alpha_0}$ values are consistent with those obtained from the means. Figure 9.9 shows that, for the global variables, the fitted values of α_s and $\overline{\alpha_0}$ are consistent with being independent of the Q-range. The non-global variables show a larger sensitivity to the Q-range possibly reflecting the poorer χ^2 of the fits.

To estimate the theoretical uncertainties for both the mean values and the differential distributions, the renormalization scale was varied by a factor of two, and studies were made of the effects of changes to μ_I and to the Milan factor. To give an indication of the uncertainties due to mass effects, the data were reanalyzed using the E-scheme. For the means, the CTEQ4 PDFS were replaced by the MRS99 set. For the differential distributions, the additional parameters p and p_s, that ensure the correct behavior of the matching and shift, were varied as shown in Table 9.7 and Table 9.8. The logarithmic rescaling factor, x_L, was changed to 1.5 [?] and the CTEQ5 PDF was used instead of MRS99.

For the determination of $\alpha_S(M_Z)$ and α_0 from the mean values of the event shapes, the main contributions to the theoretical uncertainties originate from the renormalisation scale μ_R and PC scale μ_I. Similarly, for the differential distributions, the renormalisation scale give the dominant theoretical uncertainty. However, in this case, the results are insensitive to μ_I, but are significantly dependent on the scales associated with the shape variables, the form of the matching, and the power corrections to the NLL distribution and the matching.

Table 9.7 and Table 9.8 also give the theoretical uncertainties in the fitted

$(\alpha_s(M_Z), \overline{\alpha_0})$ values. For α_s, the dominant theoretical uncertainties result from the renormalization scale and the logarithmic rescale factor. The power factors in the modification terms also give rise to significant uncertainties for all variables except $(1 - T_\gamma)$. In contrast to that found for the means, changes in the Milan factor and μ_I have no significant influence on the fitted α_s which indicates that the power correction, represented by (2.26) , gives a good representation of hadronisation effects for the differential distributions in the range used for the fits. Table 9.7 shows that, in general, all theoretical uncertainties have a magnitude of several times the Hessian fit error.

As in the case of the means, the fitted values of $(\alpha_s(M_Z), \overline{\alpha_0})$ for the differential distributions are inconsistent with one another with the non-global variables, M^2, C and $(1 - T_T)$, fitting to a lower α_s than the global variables $1 - T_\gamma$ and B_γ, irrespective of the matching scheme used. The inconsistency could be due to the binning of the differential distribution or theoretical uncertainties. An estimate of the influence of the binning is given in the final line of Table 9.7 and Table 9.8. This estimate was obtained by by fitting the data in 20 bins and adding/subtracting one bin at the low values of the shape variable where the influence of the NLL terms is greatest. For α_s, the effect of the change is a few percent for T_γ and B_γ. In contrast, the fit values for the non-global variables are significantly dependent on the fit range. The uncertainties due to the fit range and theoretical parameters preclude a meaningful determination of the average values for α_s and $\overline{\alpha_0}$ from the fits to the differential distribution.

9.3.3 Y_2 and K_{OUT}

In this section the two event-shape variables, y_2 and K_{OUT}, that have significance only if there are two jets in final state, are discussed. The analysis was made over the full phase space i.e. both the current and target regions of the Breit frame were included. In contrast to the event-shape variables previously described, y_2 is expected to have a $1/Q^2$ correction and is therefore expected to be small. Although the general form of the correction is known, the value of a_F in (2.23) has not yet been predicted. Consequently, no fit has been made, but the data have been compared to ARIADNE and NLO predictions. The distribution of y_2 and the mean of y_2 as a function of Q are shown in Fig. 9.10 together with the ARIADNE predictions at the hadron and parton levels. The figures show that ARIADNE describes well the y_2 distribution for $Q^2 > 320GeV^2$ but overestimates the means at lower Q.) ← give range

In Fig. 9.10 the y_2 distributions are compared with the NLO distribution from DISENT calculated using $\alpha_s = 0.116$. Except for the points at the lowest y_2 value for high Q, the NLO predictions describe the data well. It can be concluded that hadronisation effects are empirically small for y_2. It may be concluded that to NLO and to the accuracy of this experiment, hadronisation effects may be present at low y_2 and are otherwise similar to a change of α_s. In Fig. 9.10, the mean values of y_2 are plotted as a function of Q and compared with the NLO predictions. The agreement with the NLO predictions is good over the entire range of Q.

they are always present! say how small.

The K_{OUT} variable measures the momentum out of the event plane defined by two jets; it therefore depends on α_s^2 at lowest order. In the absence of a theoretical prediction to this order, the data are compared to ARIADNE predictions at the parton

and hadron level in Fig. 9.11. For the differential distribution, at the parton level, ARIADNE agrees well with the tail of the $K_{\rm OUT}$ distribution but peaks at a lower value than the data. Thus hadronization effects are important for this variable. The mean value of $K_{\rm OUT}/Q$ agrees well with the expectation from ARIADNE at the hadron level. In contrast, the parton level predictions lie below the data with a difference that decreases with Q again indicating the importance of hadronization effects.

9.4 Summary → Move to Conclusions Chapter?

Measurements have been made of mean values and differential distributions of the event-shape variables thrust T, broadening B, normalized jet mass M^2, C-parameter, y_2 and $K_{\rm OUT}$ using the ZEUS detector at HERA. The variables T and B were determined relative to the virtual photon axis and the thrust axis. The events were analyzed in the Breit frame for the kinematic range $0.0024 < x < 0.6$, $80 < Q^2 < 20\,480\,\mathrm{GeV}^2$ and $0.04 < y < 0.90$. The data are well described by the ARIADNE Monte Carlo model.

The Q dependence of the mean event shapes T, B, M^2 and C, have been fitted to NLO calculations from perturbative QCD using the DISASTER++ program together with the Dokshitzer-Webber non-perturbative power corrections, with the strong coupling $\alpha_s(M_Z)$ and the effective non-perturbative coupling $\overline{\alpha_0}(\mu_I)$ as free parameters.

Consistent values of α_s are obtained for the shape variables $1-T_T$, B_γ, M^2 and C, with $\overline{\alpha_0}$ values that agree to within $\pm 10\%$. For B_T, the $\overline{\alpha_0}$ value agrees with other variables, whereas the α_s does not. The variable $1-T_\gamma$ gives α_s and $\overline{\alpha_0}$ values that are inconsistent with the other variables and, in contrast to the other variables, sensitive

to the parton density used in DISASTER++. For all variables, the fitted values of α_s depend on the μ_I parameter used in the power corrections; this may be indicative of the need for higher orders in these corrections.

The program DISRESUM together with NLO calculations from DISPATCH has been used to fit the differential distributions for the event shape variables T_T, M^2, C, T_γ and B_γ for $Q^2 > 320\,\mathrm{GeV}^2$. A good description is obtained for all variables. The modified matching schemes give fitted values of α_s that are consistent with the world average. With the exception of C, the values of $\overline{\alpha_0}$ are consistent with those found from the mean values and lie within the range 0.4 - 0.5.

The power corrections for the variables y_2 and K_{OUT} have not yet been determined. For y_2 the data are well described by NLO calculations. A comparison of K_{OUT} with the parton level from ARIADNE indicates the need for substantial hadronization corrections. The variable K_{OUT} is well described by ARIADNE predictions at the hadron level.

The power correction method provides a generally successful description of the data for all event-shape variables studied. Nevertheless, the lack of consistency of the α_s and $\overline{\alpha_0}$ determinations obtained in deep inelastic scattering for the mean values in particular suggest the importance of higher-order processes that are not yet included in the model.

Very Nice Summary!

Variable	$1-T_T$	M^2	C	$1-T_\gamma$	B_γ
$\alpha_s(M_Z)$	***0.1170***	***0.1175***	***0.1192***	***0.1233***	***0.1228***
Fit error	± 0.0014	± 0.0012	± 0.0016	± 0.0011	± 0.0012
χ^2/dof	3.08	2.45	3.98	0.71	0.44
correlation	-0.71	-0.70	-0.68	-0.70	-0.73
$x_R = 0.5$	-0.0041	-0.0043	-0.0011	-0.0040	-0.0032
$x_R = 2$	$+0.0047$	$+0.0057$	$+0.0044$	$+0.0059$	$+0.0051$
$\mathcal{M} = 1.19$	$+0.0000$	-0.0000	$+0.0001$	$+0.0001$	-0.0000
$\mathcal{M} = 1.79$	-0.0000	$+0.0000$	-0.0001	-0.0002	-0.0001
$\mu_I = 1\ GeV$	$+0.0000$	-0.0001	$+0.0003$	$+0.0002$	-0.0000
$\mu_I = 4\ GeV$	-0.0001	$+0.0000$	-0.0005	-0.0003	-0.0002
$x_L = 1.5$	$+0.0048$	$+0.0047$	$+0.0052$	$+0.0025$	$+0.0040$
$x_L = 0.67$	-0.0047	-0.0049	-0.0048	-0.0035	-0.0062
$p = 2.0$	-0.0037	-0.0044	-0.0073	-0.0011	-0.0031
$p_s = 2.0$	-0.0033	-0.0029	-0.0031	-0.0015	-0.0009
E-scheme	-0.0050	$+0.0031$	-0.0090	$+0.0009$	-0.0005
PDF	0.0009	0.0008	0.0002	0.0003	0.0003
-0.5 Bins	-0.0130	-0.0094	-0.0073	-0.0013	-0.0019
+0.5 Bins	$+0.0077$	$+0.0063$	$+0.0063$	$+0.0039$	$+0.0032$

Table 9.7: Results from the Hessian fit for $\alpha_s(M_Z)$, to the differential distributions of the shape variables using DISRESUM. The second line is the total experimental error from the Hessian fit method that includes statistical and experimental systematic errors. The quoted χ^2 is that from the Hessian fit. The fourth row gives the correlation coefficients between the fitted values of $\alpha_s(M_Z)$ and $\overline{\alpha_0}$ (see next Table). The x_R, $\mathcal{M}$, μ_I, x_L, P and P_s rows give the theoretical systematic uncertainties due to variations on the renormalisation scales, the Milan factor, the lower limit for the perturbative calculation, the logarithmic rescaling factor, the matching-scheme power and the shift-power, respectively; the x_R and x_L values denote factors by which the respective values are varied. The systematic effect of using the E-scheme rather than the P-scheme and CTEQ5 PDF instead of MRST99 are given in rows 11 and 12 of the systematic errors. The final two rows show the effect of changing the fit range by half a bin at low values of the shape variable.

Variable	$1-T_T$	M^2	C	$1-T_\gamma$	B_γ
$\overline{\alpha_0}$ **(2 GeV)**	***0.4049***	***0.4598***	***0.3114***	***0.4539***	***0.4014***
Fit error	± 0.0166	± 0.0111	± 0.0166	± 0.0154	± 0.0251
$x_R = 0.5$	-0.0249	-0.0353	-0.0753	-0.0404	-0.0567
$x_R = 2$	$+0.0246$	$+0.0236$	$+0.0356$	$+0.0261$	$+0.0483$
$\mathcal{M} = 1.19$	$+0.0406$	$+0.0548$	$+0.0152$	$+0.0437$	$+0.0345$
$\mathcal{M} = 1.79$	-0.0274	-0.0360	-0.0091	-0.0287	-0.0202
$x_L = 1.5$	$+0.0232$	$+0.0338$	$+0.0285$	$+0.0477$	$+0.0713$
$x_L = 0.67$	-0.0194	-0.0237	-0.0226	-0.0390	-0.0244
$p_c = 2.0$	$+0.0200$	$+0.0296$	$+0.0597$	$+0.0127$	$+0.1145$
$p_s = 2.0$	$+0.0060$	-0.0034	$+0.0191$	$+0.0019$	-0.0139
E-scheme	$+0.0127$	$+0.0010$	$+0.0493$	$+0.0110$	-0.0037
PDF	-0.0036	-0.0034	-0.0016	-0.0029	-0.0021
-0.5 Bins	$+0.1778$	$+0.1230$	$+0.1116$	$+0.0399$	$+0.0683$
+0.5 Bins	$+0.0288$	-0.0070	-0.1039	$+0.0726$	-0.0889

Table 9.8: Fitted results for $\overline{\alpha_0}$, defined at $\mu_I = 2$ GeV using DISRESUM. Other definitions are given in the caption to Tab. ??.